ACS APPLIED MATERIALS & INTERFACES

LETTER

www.acsami.org

Controlled Self-Assembly of Metal−Organic Frameworks on Metal Nanoparticles for Efficient Synthesis of Hybrid Nanostructures

Takaaki Tsuruoka,* Hiroko Kawasaki, Hidemi Nawafune, and Kensuke Akamatsu*

Department of Nanobiochemistry, Frontiers of Innovative Research in Science and Technology (FIRST), Konan University, 7-1-20 Minatojimaminamimachi, Chuo-ku, Kobe 650-0047, Japan

Supporting Information

ABSTRACT: We report a novel approach for synthesizing inorganic nanoparticle/metal−organic frameworks (MOFs) heterostructured nanocomposites by self-assembly of MOFs on nanoparticles. This approach involves the synthesis of Au nanoparticles and preferential growth of $[Cu_3(btc)_2]_n$ frameworks consisting of Cu^{2+} ions and benzene-1,3,5-tricarboxylate (btc) on nanoparticles. Aggregates consisting of 11-mercaptoundecanoic acid (MUA)-stabilized Au nanoparticles linked by Cu^{2+} ions were necessary for preferential self-assembly of $[Cu_3(btc)_2]_n$ frameworks on the aggregates, resulting in the formation of Au nanoparticles/$[Cu_3(btc)_2]_n$ nanocomposites. The present approach was confirmed to be applicable for other hybrids consisting of Au nanoparticles and tetragonal $[Cu_2(ndc)_2(dabco)]_n$ frameworks.

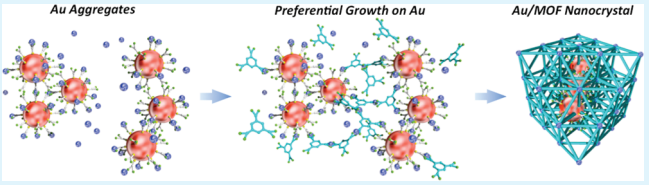

KEYWORDS: inorganic nanoparticles, metal−organic frameworks (MOFs), hybrid nanomaterials, self-assembly, Au nanoparticle, $[Cu_3(btc)_2]_n$ framework

Metal−organic frameworks (MOFs) have been intensively investigated for various applications including gas storage, separation, and catalysis because they have unique nanoscale coordination spaces.[1−4] To realize more advanced application using MOFs, the construction of multifunctional MOF composites including metal and metal oxide nanocrystals has received increasing interest because their unique gas storage, catalytic, and optical properties can be tuned by controlling the doped amount and size of nanomaterials,[5−11] and they have potential applications in heterogeneous catalysis with advantages of their molecular sieving effect,[9−11] carrier for drug delivery,[12−14] and surface-enhanced Raman spectroscopy.[16] The conventional method for MOF/nanocrystal composites synthesis involves the fabrication of MOF microcrystals by a solvothermal reaction and the in situ formation of nanocrystals from metal ions and/or organometallic compounds doped in as-prepared MOFs.[5−11,14−18] One of the major issues in synthesis of composites, however, is the need for a relatively high temperature annealing treatment to obtain nanocrystals. As nanocrystals grow inside MOFs, these in situ methods may distort or disintegrate the host framework structure. In addition, control of the size, shape, and spatial distribution of nanocrystals in MOF, which is important to obtain the inorganic nanocrystals/MOF hybrids with desired properties, is difficult. Therefore, it is critical to develp an alternative approach that enables the composite microstructure to be systematically controlled, with full potential functionality of nanocrystals and MOFs.

In this communication, we develop a new method that is based on preferential self-assembly of framework compontents on metal nanopaticles and use it to synthesize Au nanoparticles/$[Cu_3(btc)_2]_n$ heterostructured nanocomposites. The understanding of self-assembly mechanism of MOFs is of great significance for controlled synthesis of MOFs with tunable functionalities, sizes, and compositions.[19,20] Recently, the special attention has been paid on the controlled synthesis of MOFs by self-assembly on solid substrates such as MOF (MOF on MOF)[21−23] and self-assembled monolayer (SAM) functionalized substrates.[23−28] Both substrates can serve as scaffolds for the directed self-assembly of MOFs, allowing the bottom-up fabrication of core/shell and thin film MOFs. In addition, there are a few reports for self-assembly of MOF on nanomaterials, for example, carbon nanotubes,[29] iron oxide nanocrystals,[14,15] and Au nanorods.[16] Although the properties of nanomaterials/MOF composites can be readily controlled by a preferential self-assembly of MOF on as-prepared nanomaterials with desired size, shape, and composition, the growth mechanism of MOFs on nanomaterials is still a key issue in creating nanomaterials/MOF composites with desired microstructures such as nanomaterial distribution in MOF, composite size, and amount of nanomaterial loading. In the present study, we demonstrate that nanocomposites can be fabricated by growing $[Cu_3(btc)_2]_n$ on the nanoparticle surfaces, enabling simultaneous incorporation of Au nanoparticles into $[Cu_3(btc)_2]_n$, where the Au nanoparticles function as templates in the growth of $[Cu_3(btc)_2]_n$ frameworks.

The initial Au nanoparticles were prepared by the Brust method in the presence of 11-mercaptoundecanoic acid (MUA), which functions as a protective molecule.[30−32] After purifying the nanoparticles, we added an ethanol solution of copper nitrate to a

Received: July 25, 2011
Accepted: September 15, 2011
Published: September 15, 2011

suspension of MUA-stabilized Au nanoparticles in ethanol. The Au nanoparticle/$[Cu_3(btc)_2]_n$ heterostructured composites were synthesized by adding a solution of H_3btc in ethanol to the mixture of nanoparticles and copper nitrate in ethanol at 70 °C (final concentrations: Au, 1.6×10^6 mol L^{-1}; copper nitrate and H_3btc, 4.0×10^3 mol L^{-1}) (see the Supporting Information for detailed description and size histograms).

Figure 1A shows a transmission electron microscopy (TEM) image that reveals the formation of $[Cu_3(btc)_2]_n$ nanocrystals with an average diameter of 210 ± 36 nm and the incorporation of Au nanoparticles into $[Cu_3(btc)_2]_n$ nanocrystals (see Figure S1 in the Supporting Information).[33] X-ray diffraction (XRD) and thermogravimetric analysis of the resulting samples clearly demonstrates the formation of Au nanoparticle/$[Cu_3(btc)_2]_n$ composites (Figure 1C, Figures S2 and S3 in the Supporting Information): all peaks of the resulting samples are completely assigned to the peaks of $[Cu_3(btc)_2]_n$ (simulation) and Au nanoparticles. A magnified TEM and SEM images of nanocrystals reveal that the nanocrystals with an octadedral structure form (inset in Figure 1A,B and Figure S4 in the Supporting Information).[34] We conducted optical and gas-adsorption measurement of the obtained nanocomposites to investigate properties of the Au naoparticles and MOFs, respectively (Figure 2). As a result, optical absorption measurement shows clear indication of surface plasmon resonance absorption originated from Au nanoparticles, and BET measurement indicates that the nanocomposites exhibit gas adsorption−desorption properties similar to those of pure $[Cu_3(btc)_2]_n$ framework.[35] Combining these results with those characterized by TEM and XRD, the obtained nanocomposites are heterostructured nanomaterials with functions of both Au nanoparticles and MOFs. To our best knowledge, this is the first successful synthesis of MOFs nanocrystals with metal nanoparticles in solution phase, of which properties of constituent materials are preserved. It is noteworthy that the Au nanoparticles are localized around the center of the nanocrystals, which were confirmed by HRTEM observation and X-ray photoelectron spectroscopy (XPS) for Au (4f) in the purified composites (Figure 3), implying that $[Cu_3(btc)_2]_n$ grows preferential on the Au nanoparticle surface.[36]

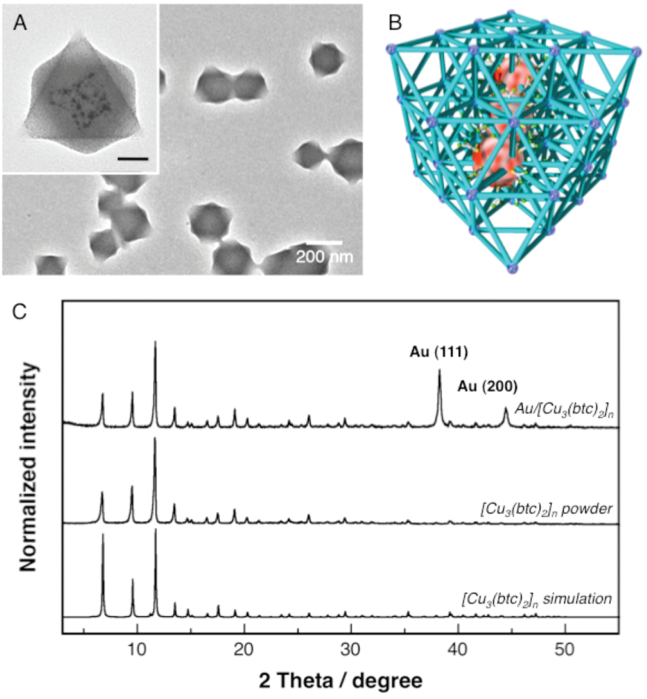

Figure 1. (A) TEM images, (B) schematic illustration, and (C) powder X-ray diffraction pattern of Au nanoparticles/$[Cu_3(btc)_2]_n$ heterostructured composites. Scale bar in the inset is 50 nm.

Figure 4 shows TEM images depicting the time course of the reaction. Before the addition of H_3btc molecules, aggregated Au nanoparticles were formed immediately on the addition of copper nitrate to the nanoparticle suspension (Figure 4A,B). This is because the Cu^{2+} ions bridge the carboxylate anions of the MUA molecules (which were generated via an ion exchange reaction), leading to clustering of Au nanoparticles. In the initial stages of the reaction (within 3 min), rounded aggregates were observed, and the original Au nanoparticles are clearly visible in the aggregates (Figure 4C,D), which implies that self-assembly of $[Cu_3(btc)_2]_n$ has mainly occurred on Au nanoparticle aggregates. XRD measurements of samples obtained during the initial stages of the reaction demonstrate the formation of $[Cu_3(btc)_2]_n$ frameworks with low crystallinities. The nanocomposite size, which is a function of the reaction time, typically reaches about 90 nm after 5 min and becomes about 180 nm after 20 min. Significantly, truncated octahedral crystals started to become visible after 5 min of the reaction (Figure 4E and F). The number

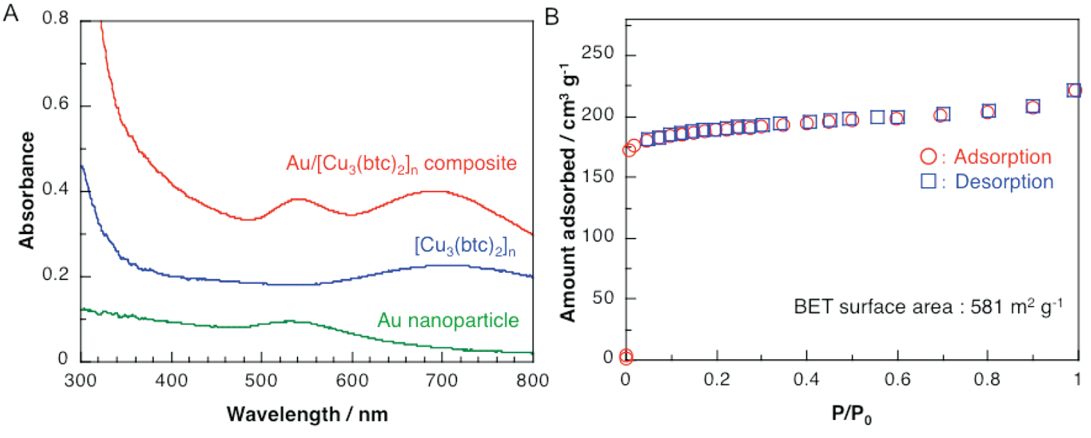

Figure 2. (A) Optical UV−vis absorption spectrum and (B) sorption isotherm for nitrogen (at 77 K) of Au nanoparticles/$[Cu_3(btc)_2]_n$ heterostructured composites.

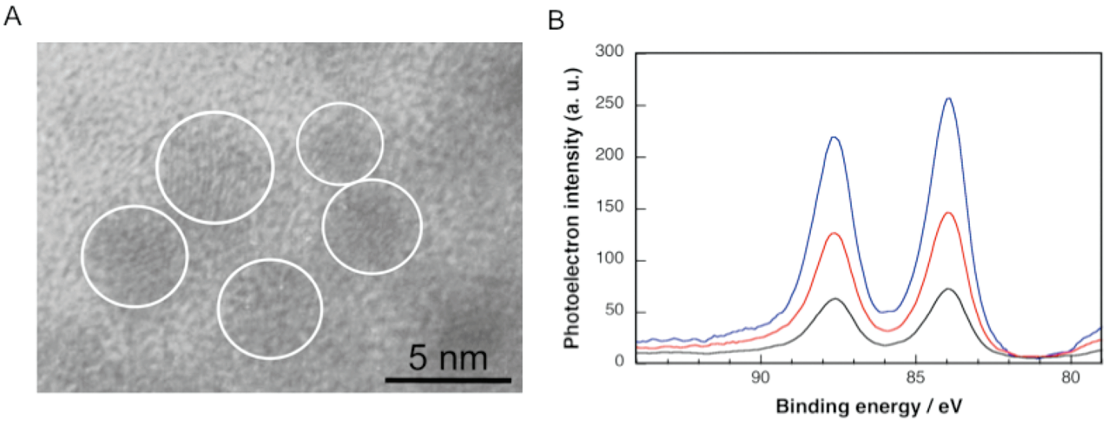

Figure 3. (A) High-resolution TEM image Au nanoparticles/$[Cu_3(btc)_2]_n$ composites. (B) XPS data for Au 4f of Au nanoparticles/$[Cu_3(btc)_2]_n$ composites dispersed on indium substrate before (black) and after Ar^+ etching at 0.3 kV for 10s (red) and 30 s (blue). Increase in photoelectron intensity with Ar^+ etching indicates that the Au nanoparticles are surrounded by $[Cu_3(btc)_2]_n$ shells.

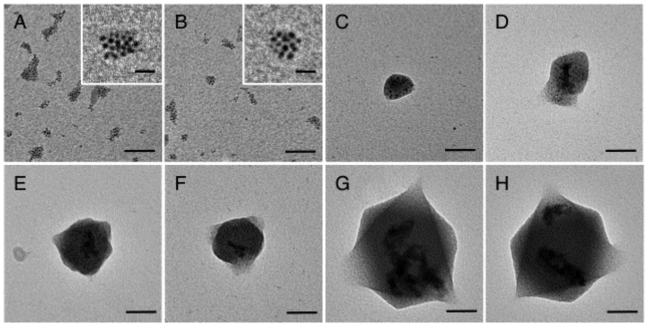

Figure 4. TEM image of Au nanoparticles/$[Cu_3(btc)_2]_n$ heterostructured composites obtained (A, B) before and (C−H) after reaction times of (C, D) 3, (E, F) 5, and (G, H) 20 min. Scale bars are 50 nm (except for those in insets, which are 10 nm).

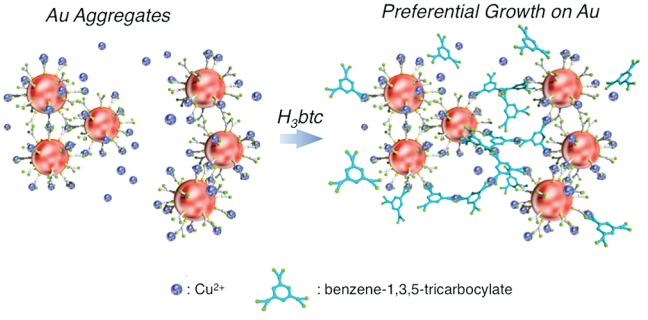

Figure 5. Schematic representation of preferential self-assembly of frameworks on aggregates of Au nanoparticles.

of these nanocrystals increased with increasing reaction time and well-structured octahedrons were observed after 20 min (Figure 4G and H). During this reaction, the XRD peaks became sharper, indicating that the growth of nanocomposites during heat treatment at 70 °C induced rearrangement of organic linkers.[19]

Importantly, we found that no Au nanoparticles in the reaction solution result in the formation of large, submicrometer-sized $[Cu_3(btc)_2]_n$ crystals. Additionally, using Au nanoparticles stabilized with 11-mercapto-1-undecanol (which includes a hydroxyl group that is a weaker trap site of Cu^{2+} ions than MUA) resulted in the Au nanoparticles being distributed only on the surfaces of relatively large $[Cu_3(btc)_2]_n$ crystals (see Figure S5 in the Supporting Information). This clearly demonstrates the importance of the electrostatic interaction between Cu ions and carboxylic acid in forming the initial precursor cores of Au nanoparticles for controlled growth of the nanocomposites.

When the same reaction was conducted using a different concentration of framework components (i.e., copper nitrate and H_3btc), while keeping the other conditions the same, the result was drastically different (see Figure S6 in the Supporting Information). Halving the concentration of the framework components relative to the Au nanoparticle concentration generated a small amount of Au nanoparticles/$[Cu_3(btc)_2]_n$ composites accompanied with a large amount of free Au nanoparticles. This is because a part of the Au nanoparticles could form aggregates due to concentration of Cu^{2+} ions. In contrast, doubling the concentration produced $[Cu_3(btc)_2]_n$ crystals without Au nanoparticles, due to the formation of Au nanoparticles bind to large amount of Cu ions which surround whole surface of Au nanoparticles (thus no aggregates form), in addition to free Cu/btc complexes. The concentration at which the Au nanoparticles aggregate lies between these two concentrations and it is a critical concentration for producing octahedral composite crystals with a high yield. As Figure 5 shows, Au nanoparticles are initially formed by Cu^{2+} ions attaching to the carboxylate anions of MUA molecules through a delicate balance of the concentration of each component. Because the trap site of Cu^{2+} ions for btc is densely localized at the aggregate surface, these aggregates can function as nuclei for further preferential, self-assembled growth of $[Cu_3(btc)_2]_n$ frameworks. Thus, the size, shape, and structure of composites could be kinetically controlled via the initial concentration of each constituent, providing a simple and general methodology for fabricating metal nanoparticle/MOF nanocomposites. This approach can be easily extended to other types of porous coordination polymers. Self-assembly of $[Cu_2(ndc)_2(dabco)]_n$ (ndc: 1,4-naphtalene dicarboxylate; dabco: 1,4-diazabicyclo[2.2.2]octane), which has a tetragonal crystal system,[19,21] results in the fabrication of Au nanoparticles/$[Cu_2(ndc)_2(dabco)]_n$ composite tetragons (see Figure S7 in the Supporting Information).

In summary, we demonstrated that preferential self-assembly of metal−organic complexes on molecular-functionalized

nanoparticles can be used to fabricate Au nanoparticles/MOF composite nanomaterials. The key to forming such nanocomposites is controlling the surface functionality of the nanoparticles and the precursor concentrations. This method can also be used to fabricate various types of nanoparticles/MOF composites that exhibit the optoelectronic properties of the nanoparticles and the molecular sieving effect of the MOFs; this is of particular importance to applications such as molecular detection using surface-enhanced Raman scattering, catalysis, and drug delivery systems.

■ ASSOCIATED CONTENT

Supporting Information. Experimental details; size and size distribution, powder X-ray diffraction measurement, thermogravimetric analysis, and SEM images of the resulting samples; TEM images of composite using Au nanoparticles stabilized with 11-mercapto-1-undecanol; effect of concentration on structure of hybrid materials; TEM images of Au nanoparticles/$[Cu_2(ndc)_2(dabco)]_n$ composites. This material is available free of charge via the Internet at http://pubs.acs.org.

■ AUTHOR INFORMATION

Corresponding Author

*E-mail: tsuruoka@center.konan-u.ac.jp (T.T.); akamatsu@center.konan-u.ac.jp. (K.A.), Japan, TEL: +81-78-303-1452, FAX: +81-78-303-1495.

■ ACKNOWLEDGMENT

The authors acknowledge Dr. Hideto Minami, Dr. Minoru Mizuhata and Mr. Taisuke Kuroda for measurement of gas sorption isotherms, TEM observation and fruitful discussions.

■ REFERENCES

(1) Yaghi, O. M.; O'Keeffe, M.; Ockwig, N. W.; Chae, H. K.; Eddaoudi, M.; Kim, J. *Nature* **2003**, *423*, 705–714.

(2) Kitagawa, S.; Kitaura, R.; Noro, S. *Angew. Chem., Int. Ed.* **2004**, *43*, 2334–2375.

(3) Férey, G.; Mellot-Draznieks, C.; Serre, C.; Millange, F. *Acc. Chem. Res.* **2005**, *38*, 217–225.

(4) Mueller, U.; Schubert, M.; Teich, F.; Puetter, H.; Schierle-Arndt, K.; Pastré, J. *J. Mater. Chem.* **2006**, *16*, 626–636.

(5) Yang, S. J.; Choi, J. Y.; Chae, H. K.; Cho, J. H.; Nahm, K. S.; Park, C. R. *Mater. Chem.* **2009**, *21*, 1893–1897.

(6) Sabo, M.; Henschel, A.; Fröde, H.; Klemm, E.; Kaskel, S. *J. Mater. Chem.* **2007**, *17*, 3827–3832.

(7) El-Shall, M. S.; Abdelsayed, V.; Khder, A. E. R. S.; Hassan, H. M. A.; El-Kaderi, H. M.; Reich, T. E. *J. Mater. Chem.* **2009**, *19*, 7625–7631.

(8) Hermannsdörfer, J; Kampe, R. *Chem.—Eur. J.* **2011**, *17*, 8071–8077.

(9) Hwang, Y. K.; Hong, D. Y.; Chang, J. S.; Jhung, S. H.; Seo, Y. K.; Kim, J.; Vimont, A.; Daturi, M.; Serre, C.; Feréy, G. *Angew. Chem., Int. Ed.* **2008**, *47*, 4144–4148.

(10) Ishida, T.; Nagaoka, M.; Akita, T.; Haruta, M. *Chem.—Eur. J.* **2008**, *14*, 8456–8460.

(11) Pan, Y.; Yuan, B.; Li, Y.; He, D. *Chem. Commun.* **2010**, *46*, 2280–2282.

(12) Horcajada, P.; Serre, C.; Vallet-Regí, M.; Sebban, M.; Taulelle, F.; Férey, G. *Angew. Chem., Int. Ed.* **2006**, *45*, 5974–5978.

(13) Horcajada, P.; Serre, C.; Maurin, G.; Ramsahye, N. A.; Balas, F.; Vallet-Regí, M.; Sebban, M.; Taulelle, F.; Férey, G. *J. Am. Chem. Soc.* **2008**, *130*, 6774–6780.

(14) Lohe, M. R.; Gedrich, K.; Freudenberg, T.; Kockrick, E.; Dellmann, T.; Kaskel, S. *Chem. Commun.* **2011**, *47*, 3075–3077.

(15) Ke, F.; Yuan, Y.-P.; Qiu, L.-G.; Shen, Y.-H.; Xie, A.-J.; Zhu, J.-F.; Tian, Z.-Y.; Zhang, L.-D. *J. Mater. Chem.* **2011**, *21*, 3843–3848.

(16) Sugikawa, K.; Furukawa, Y.; Sada, K. *Chem. Mater.* **2011**, *23*, 3131–3143.

(17) Schröder, F.; Esken, D.; Cokoja, M.; van den Berg, M. W. E.; Lebedev, O. I.; Tendeloo, G. V.; Walaszek, B.; Buntkowsky, G.; Limbach, H.-H.; Chaudret, B.; Fischer, R. A. *J. Am. Chem. Soc.* **2008**, *130*, 6119–6130.

(18) Meilikhov, M.; Yusenko, K.; Esken, D.; Turner, S.; Van Tendeloo, G.; Fischer, R. A. *Eur. J. Inorg. Chem.* **2010**, 3701–3714.

(19) Tsuruoka, T.; Furukawa, S.; Takashima, T.; Yoshida, K.; Isoda, S.; Kitagawa, S. *Angew. Chem., Int. Ed.* **2009**, *48*, 4739–4743.

(20) Diring, S.; Furukawa, S.; Takashima, Y.; Tsuruoka, T.; Kitagawa, S. *Chem. Mater.* **2010**, *22*, 4531–4538.

(21) Furukawa, S.; Hirai, K.; Nakagawa, K.; Takashima, Y.; Matsuda, R.; Tsuruoka, T.; Kondo, M.; Haruki, R.; Tanaka, D.; Sakamoto, H.; Shimomura, S.; Sakata, O.; Kitagawa, S. *Angew. Chem., Int. Ed.* **2009**, *48*, 1766–1770.

(22) Furukwa, S.; Hirai, K.; Takashima, Y.; Nakagawa, K.; Kondo, M.; Tsuruoka, T.; Sakata, O.; Kitagawa, S. *Chem. Commun.* **2009**, *45*, 5097–5099.

(23) Shekhah, O.; Hirai, K.; Wang, H.; Uehara, H.; Kondo, M.; Diring, S.; Zacher, D.; Fischer, R. A.; Sakata, O.; Kitagawa, S.; Furukawa, S.; Wöll, C. *Dalton Trans.* **2011**, *40*, 4954–4958.

(24) Hermes, S.; Schröder, F.; Chelmowski, R.; Wöll, C.; Fischer, R. A. *J. Am. Chem. Soc.* **2005**, *127*, 13744–13745.

(25) Hermes, S.; Zacher, D.; Baunemann, A.; Wöll, C.; Fischer, R. A. *Chem. Mater.* **2007**, *19*, 2168–2173.

(26) Shekhah, O.; Wang, H.; Paradinas, M.; Ocal, C.; Schüpbach, B.; Terfort, A.; Zacher, D.; Fischer, R. A.; Wöll, C. *Nat. Mater.* **2009**, *8*, 481–484.

(27) Makiura, R.; Motoyama, S.; Umemura, Y.; Yamanaka, H.; Sakata, O.; Kitagawa, H. *Nat. Mater.* **2010**, *9*, 565–571.

(28) Hinterholzinger, F.; Scherb, C.; Ahnfeldt, T.; Stock, N.; Bein, T. *Phys. Chem. Chem. Phys.* **2010**, *12*, 4515–4520.

(29) Yang, S. J.; Choi, J. Y.; Chae, H. K.; Cho, J. H.; Nahm, K. S.; Park, C. R. *Chem. Mater.* **2009**, *21*, 1893–1897.

(30) Brust, M.; Walker, M.; Bethell, D.; Schiffrin, D. J.; Whyman, R. *J. Chem. Soc., Chem. Commun.* **1994**, 801–802.

(31) Akamatsu, K.; Hasegawa, J.; Nawafune, H.; Katayama, H.; Ozawa, F. *J. Mater. Chem.* **2002**, *12*, 2862–2865.

(32) Daniel, M.-C.; Astruc, D. *Chem. Rev.* **2004**, *104*, 293–346.

(33) The average size of Au nanoparticles increases from 3.2 ± 0.7 nm to 9.5 ± 3.4 nm as shown in Figure S1 in the Supporting Information. These large of nanoparticles may be formed by coalescence of smaller nanoparticles due to partial desorption of MUA molecules on Au nanoparticles during reaction.

(34) Biemmi, E.; Scherb, C.; Bein, T. *J. Am. Chem. Soc.* **2007**, *129*, 8054–8055.

(35) BET surface area of Au nanoparticles/$[Cu_3(btc)_2]_n$ crystals was 581 $m^2\ g^{-1}$. To estimate the adsorption property of $[Cu_3(btc)_2]_n$ crystals of the composites, we calculated the weight percentage of $[Cu_3(btc)_2]_n$ crystals in the resulting composites using a molar fraction of starting materials from initial concentration of stating materials in the solution. From the BET surface area of composites and the result of calculation (weight percentage: 66.9%), the estimated BET surface area was 868 $m^2\ g^{-1}$, which is comparable to that of pure $[Cu_3(btc)_2]_n$ crystals (see Chui, S. S.-Y.; Lo, S. M.-F.; Charmant, J. P. H.; Orpen, A. G.; Williams, I. D. *Science* **1999**, *283*, 1148–1150).

(36) We tried to estimate the yield of nanocomposite. The yield of the MOF crystals including Au nanoparticles was estimated as following: one hundred crystals were counted in TEM image. A total of 91 $[Cu_3(btc)_2]_n$ crystals with Au nanoparticles were counted out of one hundred crystals. The yield was, thus, roughly estimated to be ca. 90%.